2010

Genesis of Pre-hurricane Felix (2007). Part I

Z. Wang

Genesis of Pre-hurricane Felix (2007). Part I: The Role of the Easterly Wave Critical Layer, J. Atmos. Sci., 67, 1711-1729: 2010, Z. Wang, M. T. Montgomery, and T. J. Dunkerton

Genesis of Pre–Hurricane Felix (2007). Part I: The Role of the Easterly Wave Critical Layer

ZHUO WANG

University of Illinois at Urbana–Champaign, Urbana, Illinois

M. T. MONTGOMERY

Naval Postgraduate School, Monterey, California, and NOAA/Hurricane Research Division, Miami, Florida

T. J. DUNKERTON

Naval Postgraduate School, Monterey, California, and NorthWest Research Associates, Bellevue, Washington

(Manuscript received 22 December 2009, in final form 30 December 2009)

ABSTRACT

The formation of pre–Hurricane Felix (2007) in a tropical easterly wave is examined in a two-part study using the Weather Research and Forecasting (WRF) model with a high-resolution nested grid configuration that permits the representation of cloud system processes. The simulation commences during the wave stage of the precursor African easterly-wave disturbance. Here the simulated and observed developments are compared, while in Part II of the study various large-scale analyses, physical parameterizations, and initialization times are explored to document model sensitivities.

In this first part the authors focus on the wave/vortex morphology, its interaction with the adjacent intertropical convergence zone complex, and the vorticity balance in the neighborhood of the developing storm. Analysis of the model simulation points to a bottom-up development process within the wave critical layer and supports the three new hypotheses of tropical cyclone formation proposed recently by Dunkerton, Montgomery, and Wang. It is shown also that low-level convergence associated with the ITCZ helps to enhance the wave signal and extend the ''wave pouch'' from the jet level to the top of the atmospheric boundary layer. The region of a quasi-closed Lagrangian circulation within the wave pouch provides a focal point for diabatic merger of convective vortices and their vortical remnants. The wave pouch serves also to protect the moist air inside from dry air intrusion, providing a favorable environment for sustained deep convection. Consistent with the authors' earlier findings, the tropical storm forms near the center of the wave pouch via system-scale convergence in the lower troposphere and vorticity aggregation. Components of the vorticity balance are shown to be scale dependent, with the immediate effects of cloud processes confined more closely to the storm center than the overturning Eliassen circulation induced by diabatic heating, the influence of which extends to larger radii.

1. Introduction

The problem of tropical cyclogenesis can be regarded meaningfully as a two-stage problem. The first stage is the preconditioning of the synoptic and meso-α environment, and the second stage is the construction and organization of a tropical-cyclone-scale vortex at the meso-β scale (Karyampudi and Pierce 2002). Like the components of a telescoping camera lens, these two stages distinguish processes at different spatial scales that, nevertheless, may overlap somewhat in time. The distinction is therefore primarily logical rather than chronological, underscoring the multiscale nature of tropical cyclogenesis at any instant. Many studies have focused on the second stage, and there are broadly two groups of ideas regarding this stage: (i) ''top-down'' development wherein a vortex in the midtroposphere [which presumably forms within the stratiform region of a mesoscale convective system (MCS)] somehow engenders a surface circulation by ''building downward'' from the midtroposphere and (ii) ''bottom-up'' development in which the spinup of the system-scale vortex occurs at low altitudes (below ~3 km) in association with the generation and aggregation of primarily cyclonic potential vorticity (PV)

Corresponding author address: Zhuo Wang, Department of Atmospheric Sciences, University of Illinois, Urbana, IL 61801.
E-mail: zhuowang@illinois.edu

DOI: 10.1175/2009JAS3420.1

anomalies through condensation heating in relatively downdraft-free convection. The review by Tory and Montgomery (2006) provides further discussion on these perspectives.

Hendricks et al. (2004) and Montgomery et al. (2006) proposed a vortical hot tower (VHT) route for tropical cyclone bottom-up development. The notion of a ''vortical'' hot tower generalizes the concept of a tall, protected region of undilute ascent (Riehl and Malkus 1958; Riehl and Simpson 1979; Simpson et al. 1998) to a rotating environment. Montgomery and collaborators showed that in a favorable vorticity- and moisture-rich tropical environment, VHTs quickly emerge as the dominant coherent structures and act as essential building blocks in constructing the tropical cyclone (TC) vortex via diabatic vortex merger and low-level convergence. This process occurs alongside the more familiar adiabatic merger of vortical remnants of MCSs in a prevailing cyclonic flow. From a broad scale perspective, the VHTs act collectively as a persistent thermodynamic heat forcing for the transverse circulation in the developing quasi-circular protovortex. This ''Eliassen'' forcing of the transverse circulation generates low-level convergence on the system scale, which enhances the preexisting cyclonic circulation in the lower troposphere and near the surface. The top-down versus bottom-up viewpoints have been debated in recent years, and observational evidence supporting the bottom-up route continues to accumulate (e.g., Reasor et al. 2005; Sippel et al. 2006; Houze et al. 2009). The two pathways are not mutually exclusive. It is possible that one pathway is more relevant in one region or scale than another (Halverson et al. 2007; Dunkerton et al. 2009, hereafter DMW09.).

Both groups of mesoscale theories (top-down and bottom-up) focus on the second stage of the TC formation. For the first stage, although some necessary conditions for tropical cyclone development have been known for more than four decades (e.g., warm SST, low-level cyclonic disturbance, weak vertical wind shear, and moist instability; Gray 1968), studies have not successfully answered the questions of where, when, and why a TC-scale vortex forms within a precursor synoptic-scale disturbance. This is for good reason: the wide range of spatial scales has been computationally prohibitive. Until now, only a subset of scales has been accessible, encompassing the storm domain only, while observations of tropical cyclogenesis in tropical easterly waves suggest a multiscale process (e.g., Gray 1998).

Inspired by careful study of weather analyses and discussions posted by Tropical Analysis and Forecast Branch (TAFB) forecasters at the U.S. National Hurricane Center (NHC), DMW09 developed a new framework for TC formation within the critical layer of a tropical easterly wave. Using three independent datasets—40-yr European Centre for Medium-Range Weather Forecasts Re-Analysis (ERA-40) data, Tropical Rainfall Measuring Mission (TRMM) 3B42 3-hourly precipitation data, and best-track data from the NHC—the Kelvin cat's eye within the critical layer of a tropical easterly wave was shown to be the preferred region of storm formation, located more precisely near the intersection of the wave critical latitude and trough axis. The wave critical layer is the region surrounding a nonlinear wave's critical latitude or surface in latitudinal shear flow. In the enclosed Kelvin cat's eye, particles are trapped and recirculate rather than being swept one way or the other by the surrounding latitudinal shear (DMW09). The cat's eye was hypothesized to be important to TC formation in three ways. Hypothesis 1 (H1) is that wave breaking or rollup of the cyclonic vorticity and moisture near the critical surface in the lower troposphere provides a favorable environment for vorticity aggregation leading to TC formation; hypothesis 2 (H2) that the cat's eye is a region of quasi-closed Lagrangian circulation, where air is repeatedly moistened by convection and protected to some degree from dry air intrusion, which favors a predominantly convective type of heating profile; and hypothesis 3 (H3) that the parent wave is maintained and possibly enhanced by diabatically amplified mesoscale vortices within the cat's eye. The combination of hypotheses H1–H3 was labeled the *marsupial paradigm* by DMW09 insofar as the cyclogenesis sequence is likened to the development of a marsupial infant in its mother's pouch. The ''juvenile'' protovortex is carried along and protected by the ''mother'' wave until it is strengthened into a self-sustaining entity. The cat's eye within the wave critical layer is thus dubbed the ''wave's pouch'' or simply ''pouch.'' DMW09 examined 55 named storms over the Atlantic and eastern Pacific during August–September 1998–2001, and 53 storms were shown to develop near the center of the wave's pouch as analyzed in ERA-40 data in accord with the hypotheses.[1] Using global model operational data, Wang et al. (2009) developed real-time forecast products based on the findings of DMW09 and showed that the tropical cyclogenesis location can be predicted up to three days in advance with an error less than 200 km.

DMW09 proposed an overarching framework that provides a useful roadmap for exploration of synoptic–mesoscale linkages essential to tropical cyclogenesis. In

[1] The two remaining storms also were found to develop in a region of closed circulation when the meridional component of wave propagation was accounted for, although in one of these cases the horizontal resolution of ERA-40 was barely adequate. For a complete definition of all technical terms used herein please consult DMW09 and the glossary therein.

DMW09, TRMM precipitation data were used as a proxy for deep moist convection, and it was shown that convection was persistent near the center of the wave pouch. While the TRMM data have good horizontal resolution for this purpose, the coarse-resolution reanalysis data used in that study are inadequate to investigate the mesoscale processes within the wave pouch. The objective of this study is to begin to close the gap between observationally resolvable scales (synoptic, meso-α) and infrequently sampled cloud scale processes (meso-γ, including VHTs) that operate within the trough region of tropical easterly waves equatorward of the easterly jet. Toward this end, our study (reported in two parts) explores the multiscale interaction and evolution of the parent wave and its pouch during tropical cyclogenesis for the real-case example of pre–Hurricane Felix that formed in the main development region (MDR) of the Atlantic basin during the 2007 hurricane season. Our primary aims are to answer the following three questions:

- How does the synoptic-scale circulation influence mesoscale processes in tropical cyclogenesis?
- How does a tropical depression-strength vortex form within a cold-core, lower tropospheric wave disturbance, and subsequently transition to a warm-core tropical cyclone?
- What are the relative roles of stratiform and convective processes in tropical cyclone formation and how does stratiform and convective precipitation evolve with time within the wave pouch?

In Part I of this study we address the first question and provide contextual information relevant to the second and third questions. In Wang et al. (2010, hereafter Part II) we address the latter questions in more detail and examine the formation of the warm-core structure, the roles of stratiform and convective processes in the genesis of Felix, and the sensitivity of its cyclogenesis to model physics and initialization. An outline of the remaining text of Part I is as follows. The numerical model and diagnostic tools are described in section 2. Section 3 provides a brief overview of the observed large-scale environment in which Felix formed. The formation of the wave pouch is discussed in section 4. The evolution of the pouch and the protovortex in the control run is examined in section 5, followed by discussions and conclusions in section 6.

2. Model and method

a. WRF model

The mesoscale model used in this study is the Weather Research and Forecasting (WRF) model version 3.0 (Skamarock et al. 2005). The WRF model is a fully compressible, nonhydrostatic model. In this study, we adopted a four-grid nested domain configuration with horizontal grid spacing 81, 27, 9, and 3 km, respectively. In the vertical direction, the model is resolved with 27 levels in a terrain-following, hydrostatic-pressure vertical coordinate, which is also called a mass vertical coordinate.

Felix was declared a tropical depression at 2100 UTC 31 August 2007 by the NHC. The WRF model was initialized at 0000 UTC 29 August 2007, about 3 days prior to genesis. Initial conditions and lateral boundary forcing for the control run were derived from the ECMWF 6-hourly analyses with T106 resolution (about 1.125° × 1.125°). Simulation on the innermost grid began six hours later (at 0600 UTC 29 August 2007) to allow for some model adjustment.

In the control simulation, the Kain–Fritsch scheme (Kain and Fritsch 1990) was used to represent cumulus convection in the two outer grids; in the two inner grids (9-km and 3-km resolution), cumulus convection was calculated explicitly at the grid scale. Other physics parameterizations used include WRF single-moment, six-class microphysics (Hong and Lim 2006) and the Yonsei University (YSU) planetary boundary layer scheme (Noh et al. 2003), Rapid Radiative Transfer Model (RRTM) longwave radiation scheme (Mlawer et al. 1997), and the Dudhia (1989) shortwave radiation scheme. Sensitivity tests were also carried out with different model physics or initial conditions, which are described in detail in Part II.

b. Flux form of the vorticity budget

Following Haynes and McIntyre (1987), Tory and Montgomery (2008), and Raymond et al. (1998), the flux form of the vorticity equation in the isobaric coordinates can be written as

$$\frac{\partial \eta}{\partial t} = -\nabla \cdot (\mathbf{V}'\eta) - \nabla \cdot \left(-\omega \mathbf{k} \times \frac{d\mathbf{V}'}{dp}\right) + \nabla \cdot \mathbf{R}, \tag{1}$$

where the absolute vorticity is defined as

$$\eta \equiv f + \frac{\partial v'}{\partial x} - \frac{\partial u'}{\partial y}, \tag{2}$$

ω is pressure vertical velocity, and according to DMW09 the wave relative flow is

$$\mathbf{V}' = (u', v') = \mathbf{V} - C_p \mathbf{i}, \tag{3}$$

where $\mathbf{i}$ is the unit vector in the zonal direction. The calculation of the wave propagation speed C_p is described in section 4. The last term on the right-hand side of Eq. (1) is the residual term, which includes frictional and turbulent forces (anything subgrid scale not included in the coarse-grained fields used to evaluate the vorticity tendency). The first term on the right-hand side

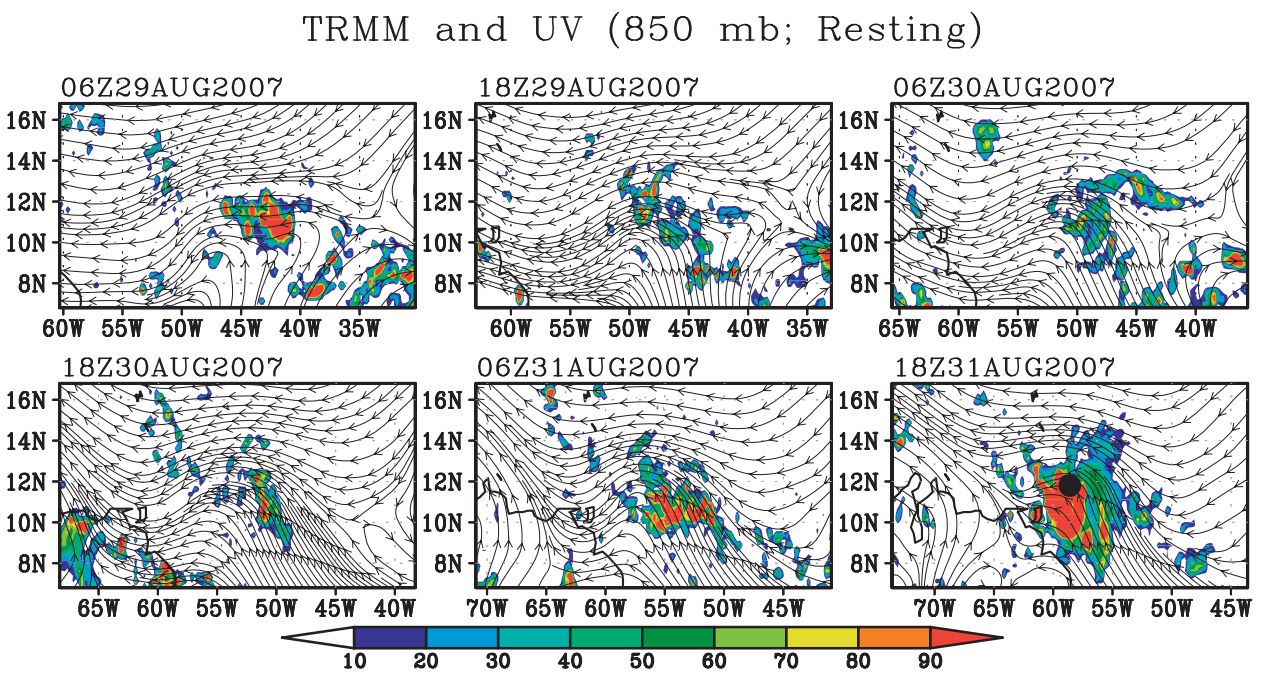

FIG. 1. Streamlines of the 2.5-day low-pass filtered 850-hPa flow from ECMWF analyses in the earth-relative frame of reference from 0600 UTC 29 Aug to 1800 UTC 31 Aug. Shading indicates TRMM 3-h accumulated precipitation (mm day^{-1}). The genesis location is indicated by the black dot in the final panel.

of Eq. (1) is the divergence of advective vorticity flux, which combines the horizontal advection and vertical stretching terms in the material form of the vorticity equation. The second term is the divergence of the nonadvective vorticity flux, which combines the vertical advection and tilting terms. Haynes and McIntyre (1987) showed that there is no net transport of vorticity across any isobaric surface, and that vorticity can be neither created nor destroyed within a layer bounded by two isobaric surfaces. Therefore, *TC genesis can be regarded as the redistribution of vorticity on the isobaric surfaces* (Tory and Montgomery 2008) provided that these surfaces do not intersect a physical boundary. In either case the residual term can be brought inside the divergence operator, as in Eq. (1), but, when isobars outcrop at the surface, a contribution to layer-mean vorticity arises from surface stress. The surface effect is limited to isobaric layers with pressure exceeding the minimum surface pressure of the storm.

3. Large-scale environment

As reported by the NHC, Felix formed within a tropical easterly wave that departed the west coast of Africa on 24 August 2007. The wave signal is clearly shown in the 2.5-day low-pass filtered (as in DMW09) 850-hPa flow field from ECMWF analyses (Fig. 1). In the earth-relative frame of reference, the wave propagated westward with an inverted-V pattern[2] (Fig. 1). Sustained convection, as indicated by TRMM 3B42 3-hourly accumulated precipitation data, occurred around the northern tip of the inverted-V pattern, and a tropical depression formed in the area of sustained convection at 2100 UTC 31 August. There was, however, no closed circulation in the filtered data at 850 hPa in the earth-relative frame, even at genesis time. Although this may be partly due to the inadequacy of the global model analyses,[3] the flow pattern in the earth-relative frame does not provide an immediate explanation for the preferred location of sustained convection and storm genesis.

For a stationary flow, streamlines are equivalent to the flow trajectories. DMW09 showed that in the frame of reference moving zonally at the same speed of the wave (hereafter the ''translated'' or ''comoving'' frame), the flow is quasi-stationary and the translated streamlines are a good approximation of the flow trajectories. To

[2] The inverted-V patterns in earth-relative streamlines and low cloud or water vapor should not be confused, as they are (dynamically and longitudinally) distinct. The schematic in Fig. 3 shows an inverted-V pattern of streamlines in the earth-relative frame.

[3] The earth-relative streamlines using unfiltered data suggest a tiny closed circulation that comes and goes during the time interval of interest (e.g., see Fig. 4). Even if this analyzed feature were real it does not represent the actual pattern of horizontal trajectories because of the time variation of the flow in this frame.

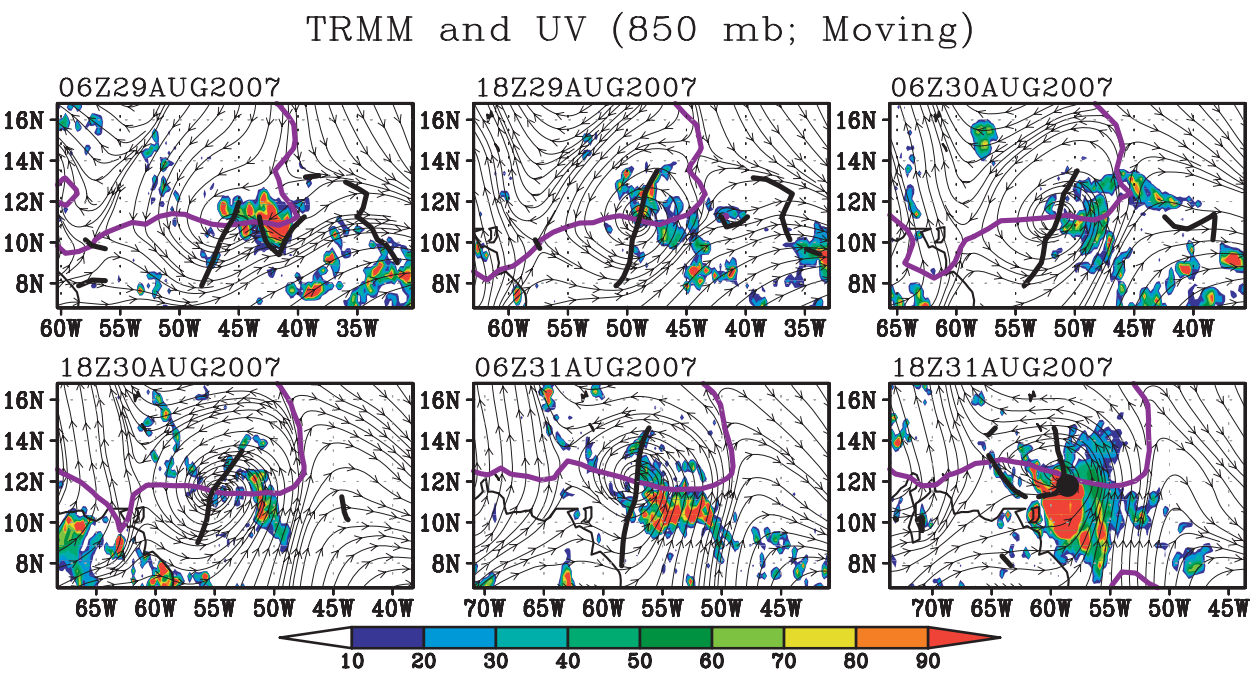

FIG. 2. As in Fig. 1 but the streamlines are displayed in the frame of reference moving westward at the zonal propagation speed of the parent wave. Isopleths of zero relative zonal flow are indicated by the purple contours, and the wave's trough axis is shown in black. The genesis location is indicated by the black dot in the final panel.

view the Lagrangian nature of the storm evolution, the streamlines are displayed in the comoving frame: in this event, the zonal wave speed is estimated at about -7.7 m s^{-1} based on the Hovmöller diagram of 700-hPa meridional wind from the ECMWF analysis. As shown in Fig. 2, a quasi-closed circulation (the *wave pouch*) is present at 850 hPa in the translated frame 2.5 days prior to genesis. Compared to the earth-relative frame, the circulation center in the translated frame shifts northward, and sustained convection is largely confined within the pouch. Genesis occurred close to the pouch center, which can be defined more precisely as the intersection of the wave critical latitude and the trough axis. This supports the hypotheses and observational findings of DMW09 that the pouch center is the preferred location for tropical cyclone formation.

What is shown for Felix in Figs. 1–2 is typical for easterly waves and can be summarized in a schematic (Fig. 3). Over the Atlantic and the eastern Pacific, tropical easterly waves play an important role in tropical cyclogenesis, and nearly 85% of the intense (or major) hurricanes originate from tropical easterly waves (e.g., Landsea 1993). A wave in the earth-relative frame of reference often appears (incorrectly) to be open, having an inverted-V pattern. Convection tends to occur around the northern tip of the inverted-V pattern along the wave trough. In the comoving frame of reference, however, a pouch may be present, although not necessarily in all cases. The formation and extent of a quasi-closed recirculation region depends, inter alia, on wave amplitude, intrinsic phase speed, and mean latitudinal shear. The pouch is a region of quasi-closed Lagrangian circulation with cyclonic rotation and weak strain/shear deformation within the wave critical layer, favoring the creation and preservation of coherent vortex structures at the meso-β scale. Its kinematic structure protects, to some extent, the convective cells inside the pouch from the hostile exterior environment [e.g., dry air associated with the Saharan air layer (SAL)]. The air within the pouch is repeatedly moistened by convection, which in turn provides a favorable environment for deep moist convection. As noted above, the pouch center is the preferred location for tropical cyclogenesis. Also indicated in Fig. 3 is a small opening of the pouch due to the divergent component of the flow, which allows influx of environmental air and vorticity. Entrainment of environmental air and its material properties may also be induced by transient flow (DMW09).

4. Formation of the wave pouch

Figure 4 shows 850-hPa streamlines and relative vorticity at the initial time of the simulation. At 0000 UTC 29 August 2007, about three days (69 h) prior to genesis, as declared by the NHC, ECMWF analyses show only weak wave signal at 850 hPa; the wave signal was stronger at

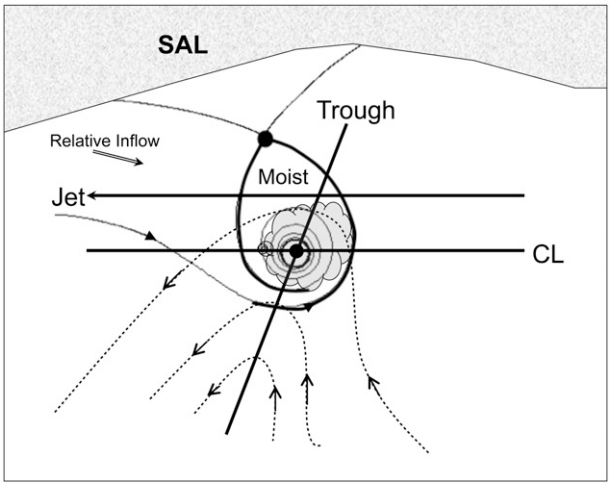

FIG. 3. Formation of a tropical storm within a wave pouch. The dashed contours represent the streamlines in the ground-based frame of reference, which usually have an inverted-V pattern. The solid streamlines delineate the wave pouch as viewed in the frame of reference moving at the same speed with the wave. The pouch can protect the mesoscale vortices inside from the hostile environment, such as dry air associated with the Saharan air layer. Deep convection (gray shading) is sustained within the pouch. Owing to convergent flow, the pouch may have an opening that allows the influx of environmental air and vorticity. The easterly jet (JET), the critical latitude (CL), and the wave trough axis (Trough) are also indicated in the schematic. The intersection of the critical latitude and the trough axis pinpoints the pouch center as the preferred location for tropical cyclogenesis.

600 hPa. The dominant feature is the intertropical convergence zone (ITCZ)—a convergence zone between the trade wind easterlies and cross-equatorial westerlies. The simulation starts from the wave stage of the precursor disturbance.

To examine the Lagrangian characteristics of the pregenesis evolution, most of the analyses in this study are carried out in the comoving frame. The propagation speed of the wave pouch is estimated from the Hovmöller diagram of the 850-hPa meridional wind v from the WRF model simulation along the latitude of storm formation (Fig. 5). The trough axis in the Hovmöller diagram is a nearly straight sloping line with the northerly flow to the west and the southerly flow to the east, suggesting a nearly constant propagation speed of about -9.8 m s^{-1}. The simulated wave has a faster phase speed than that derived from ECMWF analysis data. For analysis of model data, the simulated propagation speed is used to translate the frame of reference.

The time series of simulated minimum surface pressure and maximum 1000-hPa wind speed are shown in Fig. 6. By the end of the 72-h simulation, the surface pressure has dropped from 1013 to 985 hPa (Fig. 6a), and the maximum wind in the earth-relative frame has increased from 8 to about 33 m s^{-1} (solid line Fig. 6b). It is important to note, however, that the high wind speeds at the early stage are associated with the superposition of the parent wave and the mean easterly flow in which it is embedded. As shown in Fig. 7a, a small closed circulation has formed at 1000 hPa by 40 h (or 1500 UTC 30 August) in the earth-relative frame. Although the simulated wind speed is about 20 m s^{-1} at this time, the strongest wind is confined in the northern part of the storm, where the background easterlies exceed 6 m s^{-1}. To reduce the contribution of the background easterlies and view the wave-relative flow structure, the wind field is shown in the comoving frame of reference (Figs. 6b, 7b). The closed circulation or the wave pouch is larger and better defined (the pouch forms at 1000 hPa around 29 h) and the maximum (wave relative) wind speed is reduced to ~12 m s^{-1}. Although there is no official definition of tropical-depression-strength winds, the operational threshold effectively requires speeds of 12–15 m s^{-1} with a (presumably) closed cyclonic circulation in the lower troposphere accompanied by persistent deep convection and other characteristics in the upper troposphere resembling a mature TC (DMW09). Based on these criteria, we infer that a tropical depression may have formed during 30–40 h in the model simulation.

Formation of a quasi-closed Lagrangian circulation in the lower troposphere, accompanied (and perhaps assisted) by sufficiently intense winds in all azimuths, persistent deep convection near the center, and upper-level divergence (section 4 of DMW09) evidently constitutes the necessary criteria for a tropical depression. The historical record demonstrates that nearly all such disturbances acquire named-storm status. This is simply a testament to the accumulated operational experience of forecasters, but our suggested criteria offer better quantitative guidance and recognize the inherently Lagrangian nature of tropical cyclogenesis.

Our simulation covers the wave stage of the precursor disturbance and allows for an examination of the formation of the wave pouch in the lower troposphere. The translated streamlines, Okubo–Weiss (OW) parameter[4] (color shading), and relative vorticity (gray shading) at 600 and 850 hPa, derived from 27-km output, are shown in Fig. 8. Also shown are the local critical surface (purple

[4] The Okubo–Weiss parameter is defined herein as vorticity squared minus strain rate squared [$\mathrm{OW} = \zeta^2 - S_1^2 - S_2^2 = (V_x - U_y)^2 - (U_x - V_y)^2 - (V_x + U_y)^2$]. Assuming a scale separation between the slowly varying velocity field and the more rapidly varying field of enstrophy, McWilliams (1984) showed that positive values of OW indicate that the flow is vorticity dominant and immune from the enstrophy cascade, whereas negative values of OW indicate a strain rate-dominant flow susceptible to rapid filamentation.

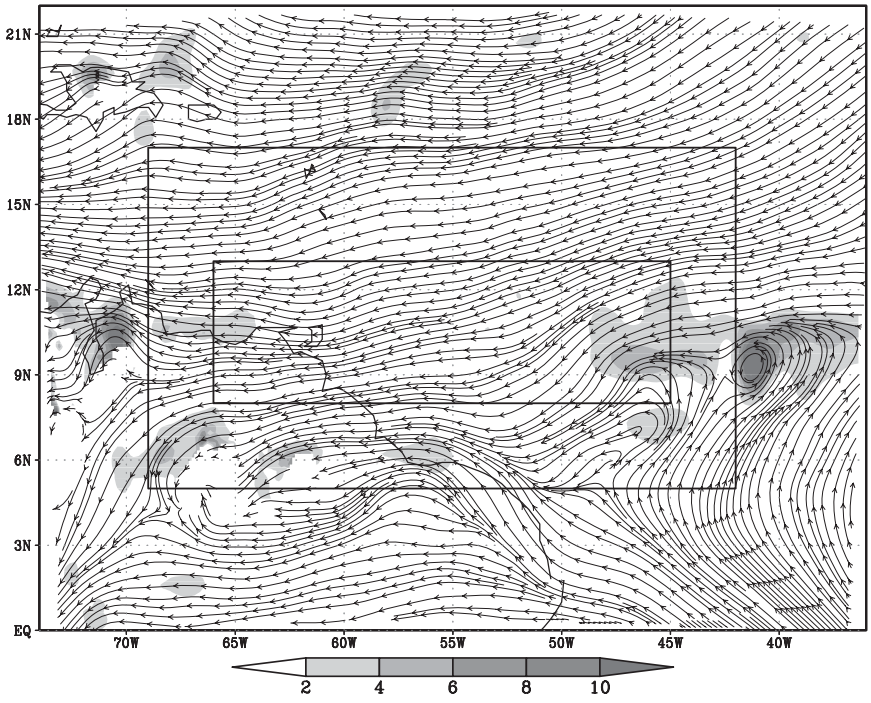

FIG. 4. Initial streamlines for the control experiment (in the resting frame of reference) and relative vorticity (shadings, 10^{-5} s^{-1}) at 850 hPa from ECMWF analysis. The rectangles represent the three inner model grids.

line) and the wave trough axis (black line). The former is defined as where the zonal flow equals the wave propagation speed, and the latter is defined as where the meridional flow is zero and relative vorticity is cyclonic. Note that the translated streamlines are intended to approximate Lagrangian trajectories and that the scalar quantities shown are invariant under a Galilean transformation.

At 600 hPa, a pouch is present from the beginning of the simulation (not shown). The OW parameter indicates that the pouch center is characterized by cyclonic rotation and weak strain/shear deformation. The wave pouch, however, is rather shallow in the beginning and does not extend down to the boundary layer. At 850 hPa, the wave signal is much weaker, and the dominant feature is the quasi-stationary ITCZ, where cross-equatorial westerlies converge with trade wind easterlies (This is better illustrated in the earth-relative frame of reference in Fig. 4; in the comoving frame of reference, the northerly component of the trade wind dominates the flow picture.) Although the ITCZ is characterized by cyclonic relative vorticity, shear vorticity is dominant in most of this region; moderate to strong cyclonic rotation (indicated

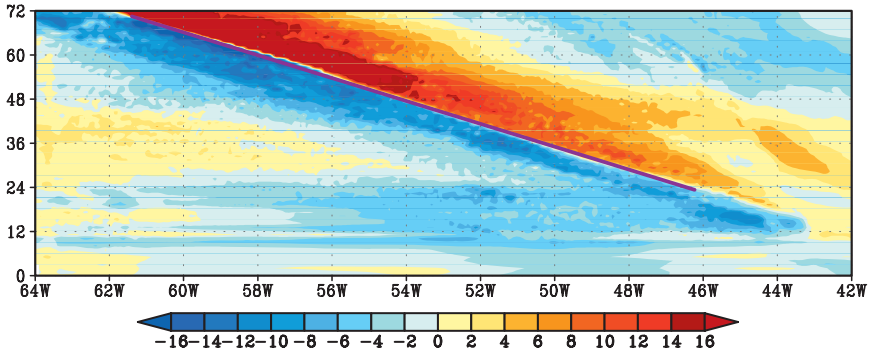

FIG. 5. Hovmöller diagrams of the 850-hPa meridional wind along 10°N as simulated by the WRF model. The purple solid line indicates the propagation of the trough axis; the estimated propagation speed is −9.8 m s^{-1}.

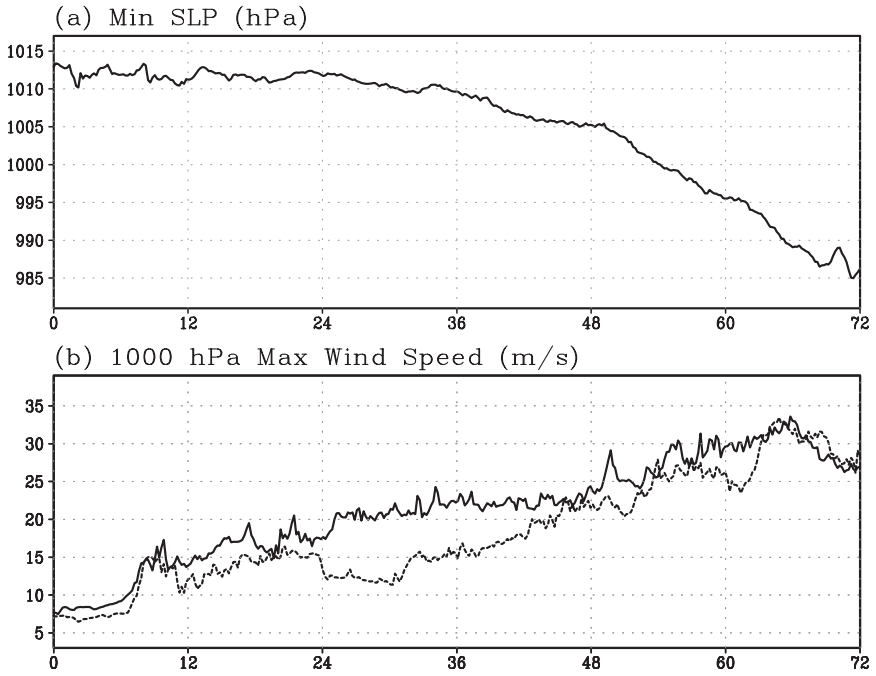

FIG. 6. Time series initialized at 0000 UTC 29 Aug of (a) the minimum surface pressure and (b) the maximum 1000-hPa wind speed in the earth-relative frame (solid line) and the comoving frame (dashed line). The wave propagation speed is -9.8 m s^{-1}. Note that the wind speed below the surface is undefined so the maximum surface wind speed is larger than that shown in (b) at the later stage. The x axis is time from 0 h (the model initialization time, 0000 UTC 29 Aug) to 72 h.

by large positive values of the OW parameter) is found only in a few patches at 9 h. There is no well-defined closed circulation at 850 hPa until 21 h. The 600-hPa wave pouch propagates along the underlying band of positive cyclonic relative vorticity, which we loosely associate with a deformed ITCZ at 15 h, and the 850-hPa maximum OW occurs within the ITCZ just below the 600-hPa pouch, suggesting that the strong OW parameter at this level may be due to the interaction between the easterly wave and the underlying ITCZ. A pouch forms at 850 hPa in the area of strong cyclonic rotation by 21 h. It is centered at the intersection of the wave trough axis and the local critical surface and is vertically aligned with the pouch at 600 hPa. While the ITCZ remains nearly stationary to the east, the wave pouch propagates westward and eventually becomes detached from the ITCZ.

Figure 8 may represent one of the scenarios by which a wave pouch extends downward to the boundary layer. Tropical easterly waves usually reach their maximum intensity around 600–700 hPa (the jet level) over the central and eastern Atlantic, while the ITCZ is confined mostly within the atmospheric boundary layer. It is plausible that convergence within the ITCZ enhances the low-level vorticity associated with the easterly wave and creates a deeper pouch structure extending to lower levels below the jet maximum. Since a convectively active pouch obtains moisture mainly from the boundary layer, a pouch extending to the boundary layer helps to keep (within the pouch) whatever moisture is lofted by deep convection into the free atmosphere, thereby creating a favorable environment for sustained convection, midlevel moistening, and further development.

It is possible to view the vertical interaction between lower-tropospheric easterly waves and near-surface ITCZ features in a complementary way, noting that the ITCZ is a region of frequent deep convection, low-level cyclonic vorticity and convergence, and abundant moisture. Midlevel mesoscale convective vortices are also prevalent here (DMW09) according to forecaster experience. However, tropical cyclogenesis is not (Dunkerton 2006) unless assisted by other processes: notably tropical waves and their critical-layer pouch above the boundary layer, which can be seen to provide a safe haven for moisture entrained horizontally from the ITCZ by the wave itself, or transported vertically by convection within the cat's eye. Simply put, the easterly wave pouch creates conditions favorable for amplification of curvature vorticity (in the comoving frame) and upward extension of the ITCZ convergence from the boundary layer to the interior.

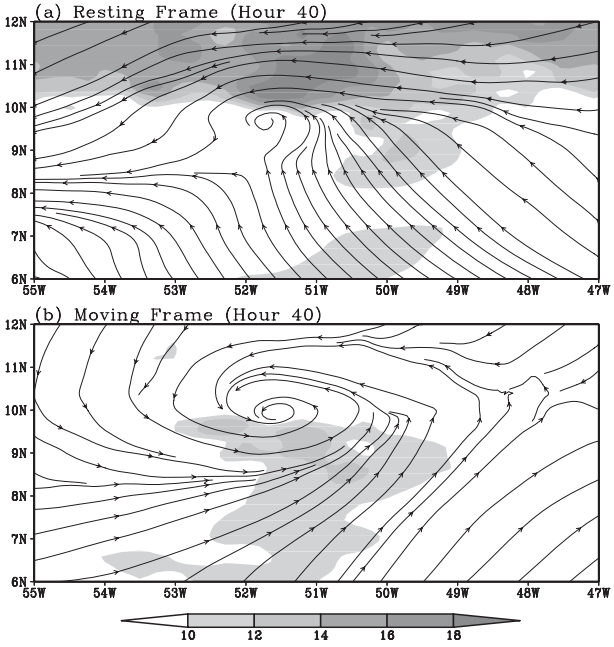

FIG. 7. The 1000-hPa streamlines and wind speed (shading, m s^{-1}) for (top) the earth-relative and (bottom) the wave-relative flow. Note that for the time shown (40 h) the 1000-hPa pressure level does not yet intersect the physical surface.

Another role of the oceanic ITCZ is to promote large-scale hydrodynamic instability, resulting in the excitation of slower easterly waves and amplification of ''teardrop'' cyclonic gyres (Hack et al. 1989; Wang and Magnusdottir 2005). Simultaneous development of multiple gyres is possible via this subpathway for TC genesis (DMW09), but in reality this instability is *local in longitude* and may involve either (i) detachment or westward motion of a closed circulation emanating from a vortex strip (as in Felix and other Atlantic MDR cases), (ii) interaction of easterly waves incident on a monsoon trough or quasi-stationary frontal zone to their west (as in the western Caribbean, Gulf of Mexico, and western Pacific), or (iii) ''tip rollup'' of vorticity filaments extending into the tropics from higher latitudes (as in the central and western oceans).

5. Evolution of the wave pouch and the protovortex

To illustrate the protection of the moist air mass (by the wave pouch) from dry air intrusion, the evolution of saturation fraction (vertically averaged relative humidity from the surface to 500 hPa) superimposed on the translated streamlines is shown in Fig. 9. Although air to the north and south of the pouch is relatively dry, the air inside the pouch is largely isolated from dry air outside (except for a weak convergence in the southwest quadrant of the pouch) and remains moist. This moist air mass is carried by the wave pouch and propagates westward. The high saturation fraction (>90%) inside the pouch indicates a nearly saturated condition of the middle and lower troposphere, which favors moist deep convection. The areal extent of high saturation fraction and maximum values of this quantity appear to increase somewhat with time, suggesting additional moistening of the pouch by deep convection therein (DMW09).

Aside from this in situ moistening, the pattern is strikingly clear: the parent wave resides on, and deforms poleward, the underlying ITCZ (Dunkerton 2006). Their combination may be likened to a large-scale *breaking wave* with dramatic cyclonic curling around the wave pouch, straining the original moist filament to the east, while entraining one or two moist filaments from the west. As noted in another MDR case by DMW09, some of the latter moisture may escape to join the eastern filament while the remaining part is drawn toward the gyre center by low-level convergence. The moisture in the filament finds itself in a region of negative OW (unfavorable for development) while some of the entrained moisture approaches the region of positive OW near the center (favorable for development). This wrap-up initially occurs slightly to the south and east of the exact center. As shown next, we find persistent deep convection in the same azimuth, slightly off center.

a. Mesoscale evolution within the pouch

Turning attention to the mesoscale developments, the 850-hPa OW parameter and precipitation superimposed on the translated streamlines from 24 to 52 h are shown in Figs. 10 and 11, respectively. The areas of strong cyclonic vorticity and weak deformation generally coincide with the areas of heavy precipitation and are associated with precursory vortical hot towers (VHTs). The horizontal scale of the VHTs is approximately 10 km, with maximum vertical velocity up to 20 m s^{-1}, consistent with Hendricks et al. (2004). Before 36 h, VHTs are most populated in the northern part of the wave pouch where moisture is abundant (see Fig. 9). VHTs begin to emerge in the southern part of the pouch after 36 h, accompanied by an increase of saturation fraction in the southern part. The VHTs and their vortical remnants merge and move toward the center of the pouch, and form one dominant vortex of stronger intensity and a larger horizontal scale at the pouch center. The formation of the tropical depression vortex at the pouch center is consistent with what is found in the real atmosphere (DMW09; Wang et al. 2009) and in an idealized high-resolution simulation (Montgomery et al. 2009). Figures 9–11 suggest that the pouch, with abundant moisture and strong cyclonic rotation, provides a favorable environment for VHT formation and is also a focal point for vorticity aggregation.

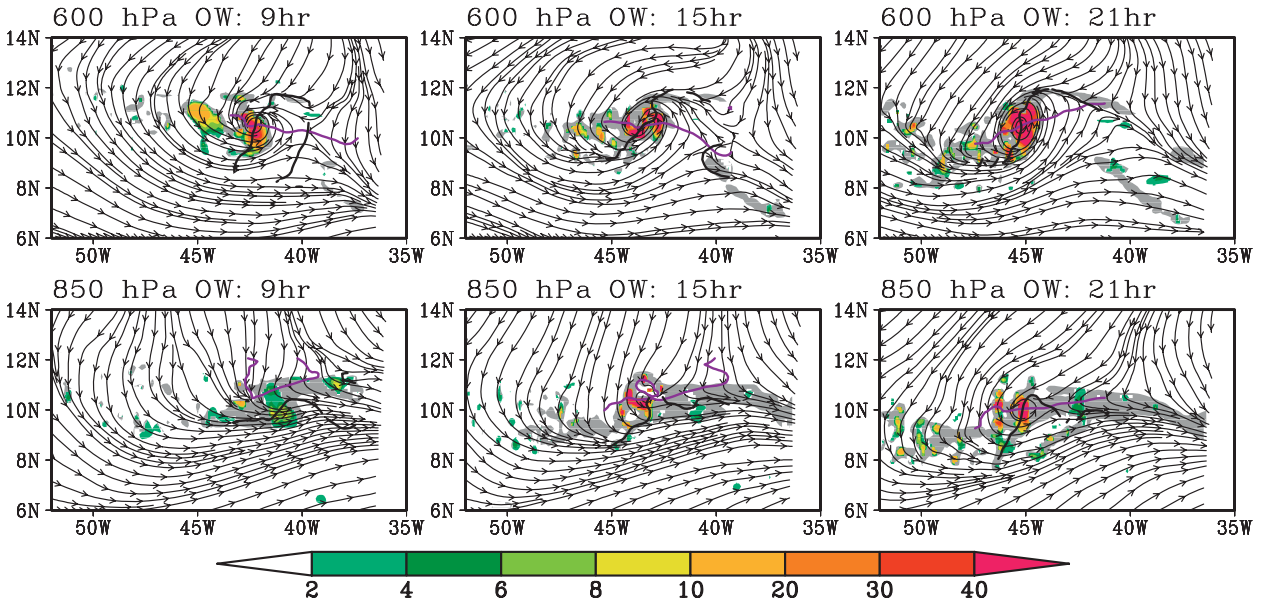

FIG. 8. The (top) 600-hPa and (bottom) 850-hPa streamlines and OW parameter (color shading, 10^{-9} s^{-2}) in the moving frame of reference (translation speed -9.8 m s^{-1}) from 9 to 21 h. The gray shading indicates the area with cyclonic relative vorticity greater than 5×10^{-5} s^{-1}. The black curve represents the wave trough axis and the purple curve is the local wave critical surface. (All fields are from the model grid with 27-km resolution.)

VHTs are the meso-γ building blocks of the meso-β hurricane monolith; their horizontal scale is generally too small, and temporal duration too short, to account for tropical depression formation and subsequent intensification to a tropical cyclone. Development entails formation of (for lack of a better term) "meso-$\gamma\beta$ clumps" of vorticity straddling the artificial boundary between these two mesoscale categories. It is possible that individual VHTs experience either a random (stochastic) or coherent (deterministic) relationship with these larger and more persistent remnants of prior VHT activity and upscale cascade. Adiabatic aggregation is also possible and is likely to continue near the exact center of the wave pouch even when deep moist convection is absent from the immediate neighborhood (or tens of kilometers away), as seen by careful inspection of these and later figures. This behavior provides a strong endorsement of the first hypothesis (H1) of DMW09, showing that the pouch regulates not only the thermodynamic aspects of moisture transport and deep moist convection (H2) but also the precise *location* of vorticity substance concentration by diabatic and adiabatic processes near the pouch center.

The deterministic feature of the genesis location is in sharp contrast with the unpredictable nature of convective processes and implies a "guiding hand" from larger to smaller scales—that is, an influence of the synoptic-scale (tropical easterly wave) or meso-α scale (the pouch) circulations on the upscale vorticity aggregation from meso-γ to meso-β scale. This large-scale influence determines primarily the genesis location (somewhere along the critical latitude's isotach) rather than the genesis time, which is more subject to the vagaries of upscale aggregation and, therefore, inherently less predictable. A priori knowledge of wave propagation can be expected to improve predictive skill of the genesis location as a locus of points around the intersection of the critical latitude and the wave trough axis. The underlying dynamical reasons were outlined in DMW09 (also in Montgomery et al. 2009 and Wang et al. 2009) and are further demonstrated in our simulations of Felix (here and in Part II). As shown in Figs. 8 and 10, the pouch center is characterized by strong rotation and weak strain/shear deformation (large positive values of OW), which hinders enstrophy cascade and favors upscale vorticity aggregation. Vorticity aggregation can in turn enhance cyclonic rotation around the pouch center and accelerate further aggregation of vorticity at this location (aka "sweet spot"). Previous studies have shown that, in an environment without external forcing, the turbulent two-dimensional flow has a tendency to form finite-amplitude coherent structures via vortex merger (e.g., McWilliams 1984). In a region of enhanced cyclonic vorticity, cyclonic vortices tend to move up the background vorticity gradient (toward the pouch center) and anticyclonic vortices tend to move down the background vorticity gradient (away from the pouch center) (Montgomery and Enagonio 1998; Schecter and Dubin 1999). Hendricks et al. (2004) compared the merger of two moist vortices in the fifth-generation Pennsylvania State

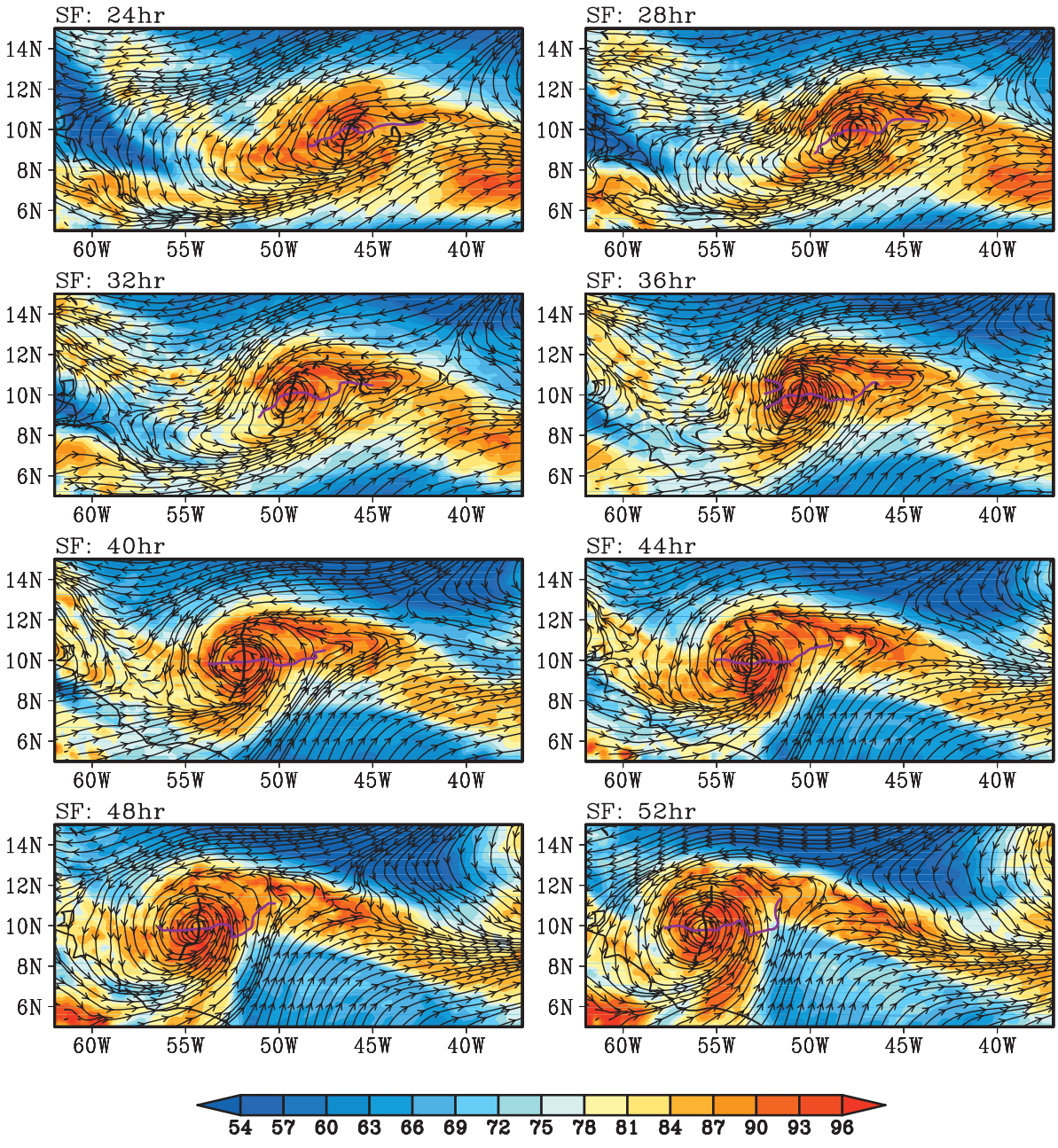

FIG. 9. The 850-hPa translated streamlines and saturation fraction (shading, %) from hour 24 to 52. All fields are from the model grid with 27-km resolution. The range of longitudes displayed is held fixed to emphasize the change of flow topology (more circular flow in the wave pouch, and more southerly monsoon flow behind it) and increasing detachment of the wave pouch from the ITCZ complex to the east. These changes resemble a steepening surface wave.

University–National Center for Atmospheric Research Mesoscale Model (MM5) and the merger of two dry vortices in a shallow-water primitive equation model. They found that in the shallow-water model (without mass sources and sinks representing the convective circulation component) the merger is slower and leads to a weaker vortex at a different location compared to the MM5 simulation. It stands to reason that the system-scale convergent flow in our simulation (Eliassen azimuthally averaged overturning circulation) accelerates the merger of remnant convective vortices and favors the development of the protovortex near the pouch center.

To understand storm formation in the Lagrangian point of view, the evolution of divergence, vorticity, relative humidity, and pseudoequivalent potential temperature θ_e (Bolton 1980) are examined following the westward

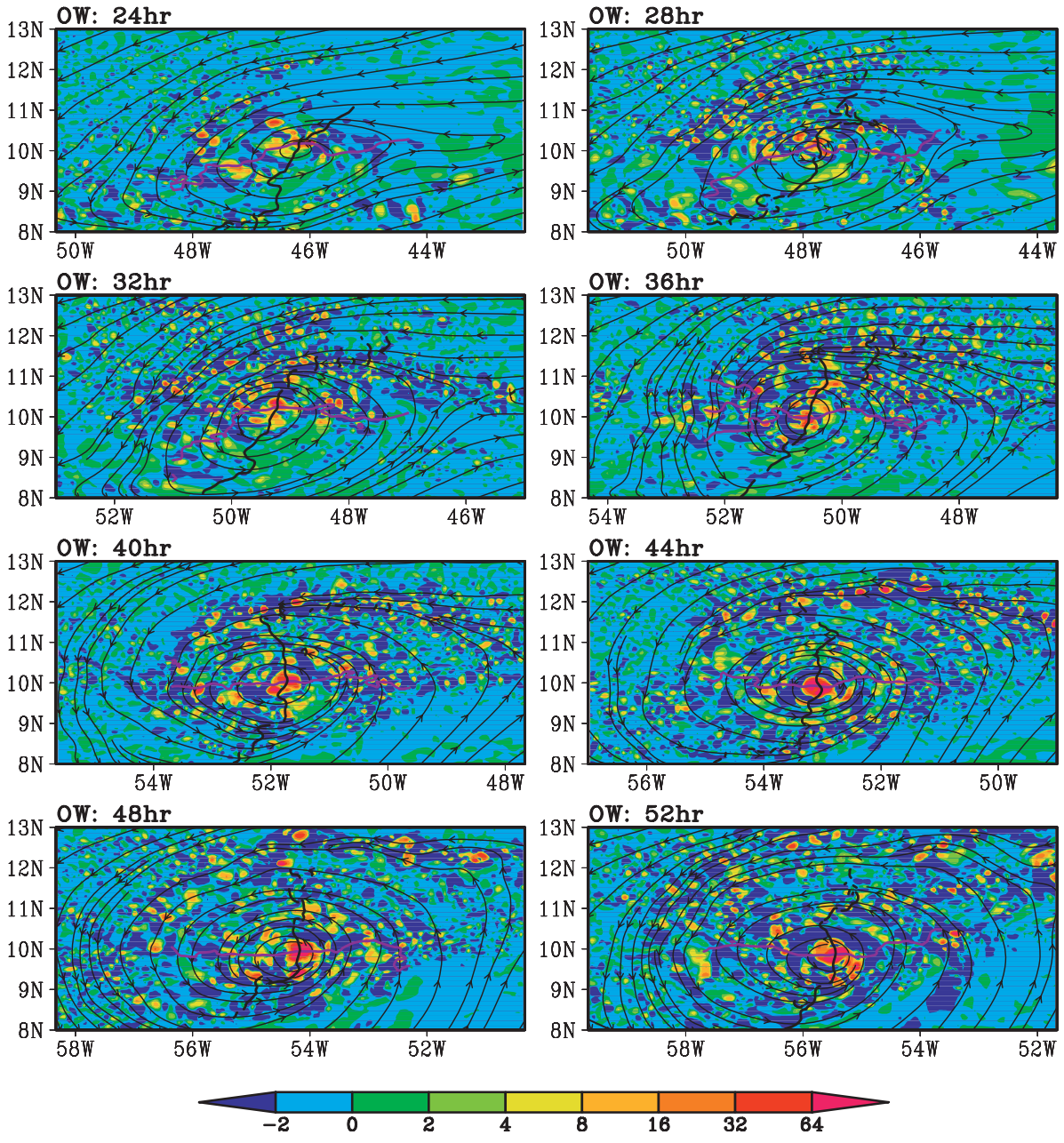

FIG. 10. Translated streamlines and OW (shading, 10^{-8} s^{-2}) at 850 hPa from hour 24 to hour 52. (OW is derived from 3-km resolution grid output.)

movement of the wave pouch. The track of the pouch is determined by manually picking the center of the closed circulation in the comoving frame of reference. The pouch track is nearly zonal and follows closely the -10 m s^{-1} zonal wind isotachs (not shown)— that is, the critical surface—which is consistent with the findings of Wang et al. (2009) using the GFS forecasts.

The time–vertical cross sections of the divergence, relative vorticity, relative humidity, and equivalent potential temperature following the pouch center during 22–72 h are shown in Figs. 12a–d. All fields were derived from the innermost grid with a 3-km horizontal resolution and 12-min time interval. They were then averaged in a 2° longitude by 2° latitude box following the propagation of the pouch. What is shown in Fig. 12 can therefore be regarded as the variations of fluid properties within the pouch, a Lagrangian coherent structure or "cat's eye" in the tropical wave critical layer.

The evolution of divergence following the wave pouch is shown in Fig. 12a. Before 24 h, the divergence profile

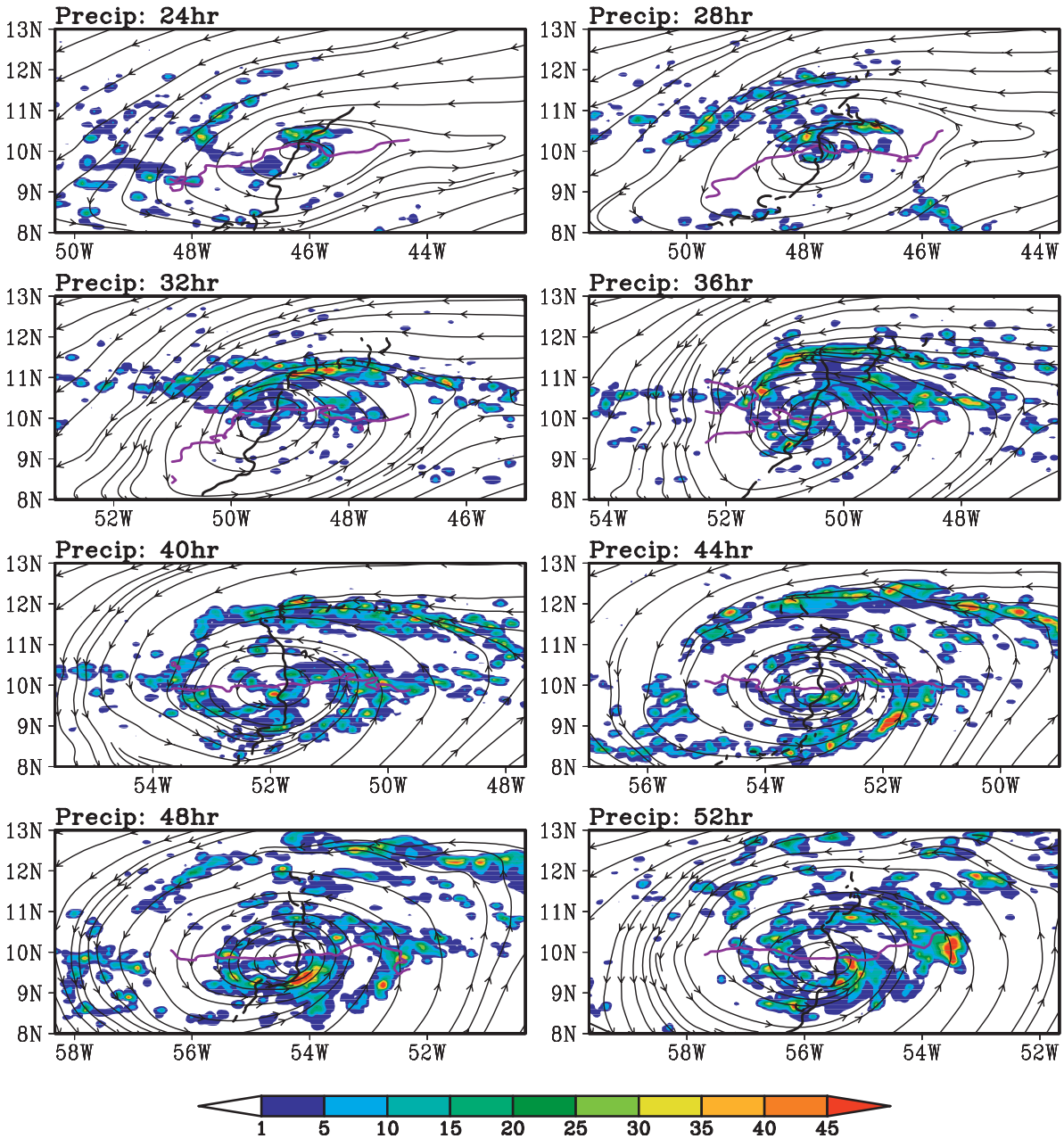

FIG. 11. Precipitation (shading, mm h^{-1}) and 850-hPa translated streamlines from hour 24 to 52. (Precipitation is from the 3-km resolution grid output.)

is consistent with a mix of the typical stratiform and convective divergence profiles, with weak divergence near the surface, strong divergence in the upper level, and convergence in the middle and lower troposphere. After 24 h, the convergence profile becomes dominantly convective, with strong low-level convergence and upper-level divergence. The low-level convergence can effectively amplify the low-level vorticity. This is consistent with Tory and Montgomery (2006) and Tory et al. (2006), which suggests that genesis involves a transition from a mean stratiform divergence profile (SDP) (Mapes and Houze 1995) to a mean convective divergence profile (CDP) (Raymond et al. 1998).

The evolution of vorticity following the pouch is shown in Fig. 12b. At the beginning of the calculation, the vorticity maximum is located at the jet level (600–700 hPa), consistent with the temperature field discussed in Part II (see Fig. 1 in Part II). The vorticity maximum gradually

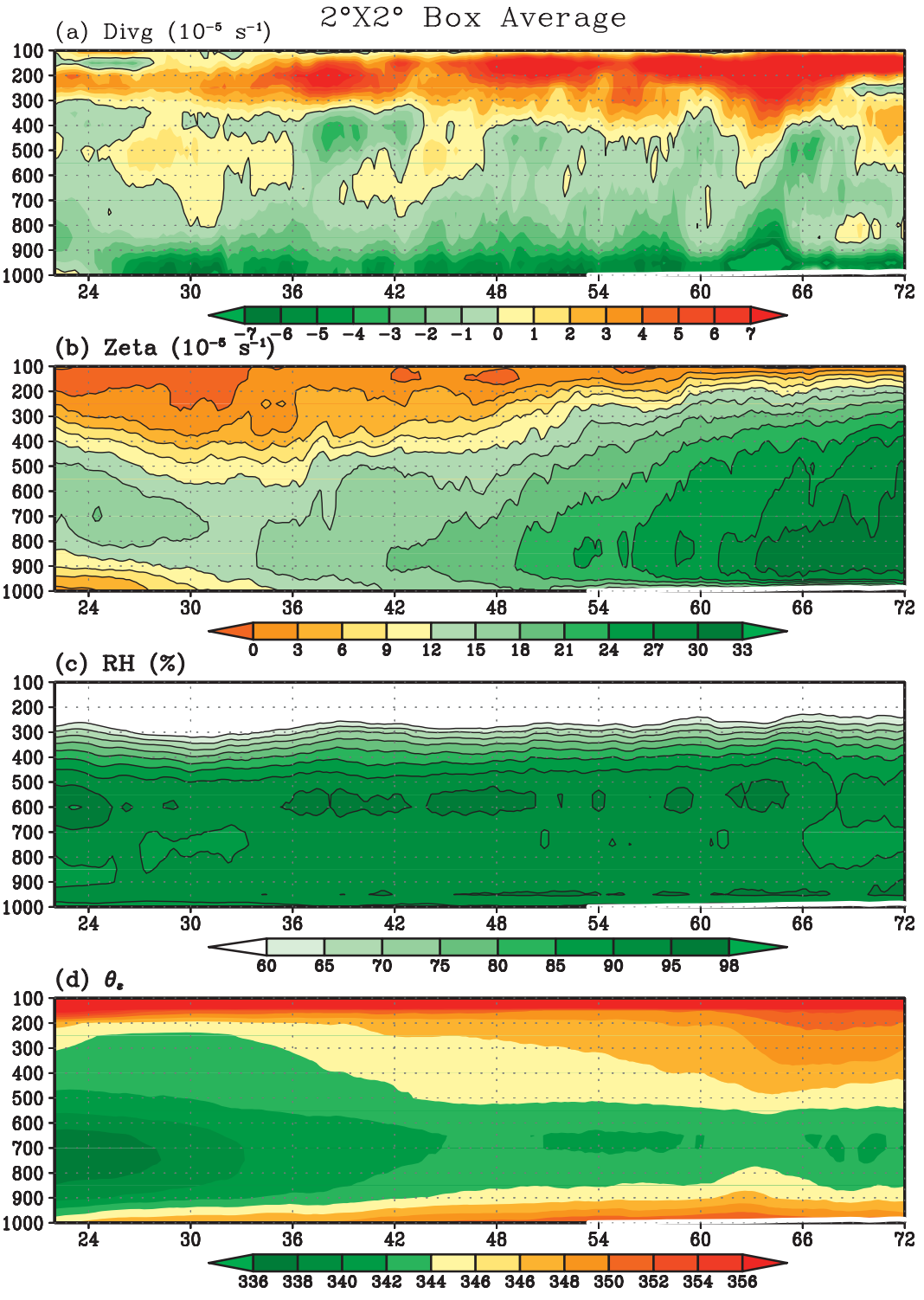

FIG. 12. Vertical distribution of the 2° × 2° box averages of (a) divergence (10^{-5} s^{-1}), (b) relative vorticity (10^{-5} s^{-1}), (c) relative humidity (%), and (d) θ_e (K) following the wave pouch center from hour 22 to 72. The abscissa is time (h), and the ordinate is pressure (hPa) (values below the surface are masked out from hour 53 to 72).

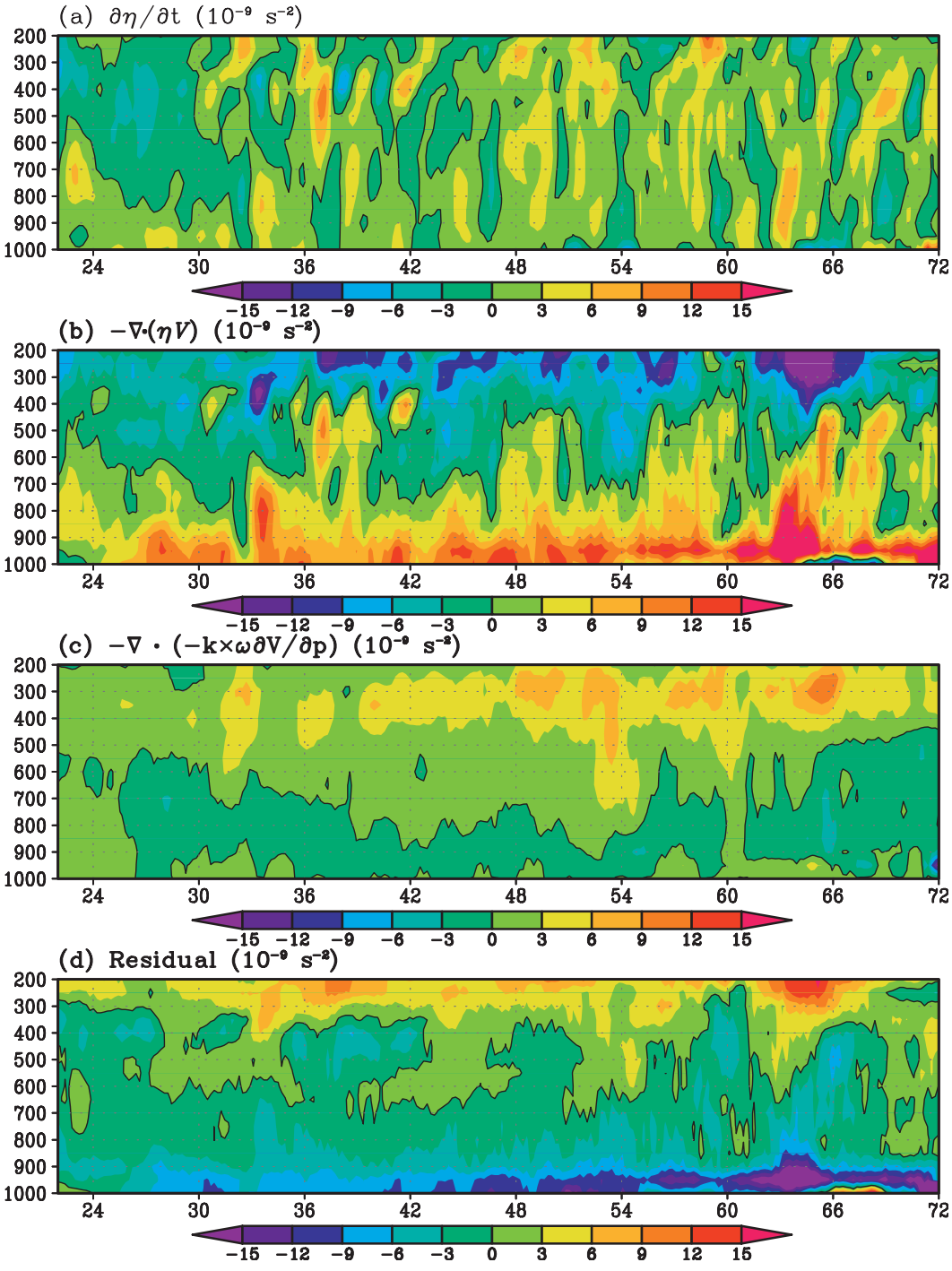

FIG. 13. Vorticity budget averaged in a 2° × 2° box following the wave pouch center from hour 22 to 72: (a) vorticity tendency, (b) convergence of the advective vorticity flux, (c) convergence of the nonadvective vorticity flux, and (d) the residual term. The units are 10^{-9} s^{-2}. Black curves are the zero contours. The abscissa is time (h), and the ordinate is pressure (hPa).

extends to the surface and descends to 900 hPa by 42 h. Meanwhile, vorticity at the middle level (~500 hPa) weakens first and then increases *after* the near-surface maximum is established. Note how this sequence of events differs from the top-down type of development proposed by Ritchie and Holland (1997). In their scenario, intensification of the low-level circulation is due to the downward extension of a midlevel vortex that results

from the merger of multiple midlevel vortices, and thus the intensification of the low-level circulation should be preceded, or at least accompanied, by the intensification, instead of weakening, of the midlevel circulation. Figure 12b shows that the intensification of the low-level circulation is preceded by low-level convergence. The vorticity budget analysis (Fig. 13) shows that the increase of low-level vorticity is due to in situ stretching instead of vertical advection from above. In this regard, it is important to recall (as noted above) that there can be no net transport of vorticity substance between isobaric layers that do not intersect the surface.

Vertical cross sections of vorticity and divergence have been constructed using ECMWF analyses in a $3^\circ \times 3^\circ$ box, which show a similar picture: the low-level convergence precedes the intensification of the near-surface cyclonic circulation. This suggests that the establishment of a convective divergence profile may be a useful predictor for genesis.

The evolution of relative humidity is shown in Fig. 12c. The pouch is relatively moist from the surface to 400 hPa from the beginning of the simulation and does not exhibit any significant change. The evolution of equivalent potential temperature following the pouch is shown in Fig. 12d. As the air column is moistened by deep convection, equivalent potential temperature increases gradually in time from the surface to the upper troposphere. However, a minimum remains around 700 hPa, which indicates the potential instability of the lower troposphere. As discussed by Tory and Montgomery (2008) the downdraft convective available potential energy (DCAPE) (Emanuel 1994), which measures the evaporative downdraft potential of a parcel, can be separated into two parts: unsaturated DCAPE and saturated DCAPE. The former can be eliminated via saturation of the air column and the latter can be reduced with the static stabilization of the atmosphere. The potential instability in the lower troposphere suggests that convection is not completely downdraft free, even at the later stage of the simulation, which is consistent with Nolan (2007). Our diagnosis in Part II (see Fig. 4 in Part II) suggests that the areal-averaged downdrafts associated with stratiform processes actually increase in time. The lesson here is that *the convective updrafts and low-level convergence remain locally dominant near the protostorm center* despite the stratiform processes that accompany the convection. It stands to reason, then, that the downward import of low entropy air into the boundary layer does not overcome the positive entropy flux from the ocean surface. As suggested by Montgomery et al. (2006), cold pools of equivalent potential temperature created by downdrafts tend to be confined laterally by the local vertical rotation and the convergent inflow near the surface; convection can be triggered at the gust front boundaries as air parcels with high θ_e are lifted. New convection can also be triggered by unbalanced motions along preexisting vortical boundaries (DMW09).

b. Vertical vorticity budget within the pouch

To better understand the processes that are responsible for the spinup of the low-level circulation, the vorticity budget analysis is done according to Eq. (1) (Fig. 13). Each term is evaluated using the 3-km resolution output with a 12-min time interval and averaged in a $2^\circ \times 2^\circ$ box as in Fig. 12. A 1-h running mean is then applied to reduce high-frequency fluctuations.

From 22 to 33 h, the vorticity tendency is positive in the lower troposphere and negative in the middle troposphere (Fig. 13a), which is consistent with the vorticity maximum descending from the jet level to the top of the planetary boundary layer (Fig. 12b). After 33 h, the overall pattern is dominated by mostly positive tendencies from 1000 to 200 hPa, corresponding to the intensification and deepening of the cyclonic vortex. The advective term, which combines the horizontal advection and the vortex stretching, makes the major contribution to the positive tendency in the lower to middle troposphere (Fig. 13b). Its pattern largely agrees with the pattern of divergence (Fig. 12a), with positive tendency associated with the low-level convergence and negative tendency associated with the upper-level divergence. This implies a dominant role of the stretching effect in spinning up the low-level circulation, including the apparent ''bringing down'' of the initial vorticity maximum from the jet level ($\sim$600 hPa).

The nonadvective term is weak in the middle and lower troposphere but contributes to the positive vorticity tendency in the upper troposphere. The residual term is characterized by the negative tendency near the surface and positive tendency near the tropopause. The former can be attributed to surface friction. Friction and friction-induced transverse circulation are the major cause of spindown. The frictional spindown effect is more than offset by the heating-induced convergence, and the net tendency is largely positive in the boundary layer.

To understand further the factors that contribute to the surface spinup near the center of the pouch, it is helpful to recall that both friction and diabatic heating contribute to the azimuthally averaged inflow near the surface (e.g., Shapiro and Willoughby 1982). During the genesis stage, the near-surface inflow that spins up the surface circulation is due primarily to deep convective processes and the corresponding mean diabatic forcing that drives the transverse circulation in the Eliassen balanced vortex model (Montgomery et al. 2006). We recall also that low-level convergence is a characteristic feature of the convective divergence profile. It would thus seem logical to

conclude that the deep convective processes are the main contributor to the surface spinup during the simulated genesis of Felix. The evolution of stratiform and deep convective precipitation and their respective contribution to the formation of Felix is examined in Part II of this study.

c. *Sensitivity of the vorticity budget analysis to the size of the box used for areal average*

In the vorticity budget analysis, the divergence of the advective and nonadvective vorticity fluxes is calculated and averaged in a $2° \times 2°$ box. According to the Stokes theorem, the areal average is equivalent to a line integral of the correspondent flux along the box boundary; that is,

$$\frac{\iint -\nabla \cdot (\mathbf{V}'\eta)dxdy}{\iint dxdy} = \frac{\oint -(\mathbf{V}'\eta \cdot \mathbf{n})dl}{\iint dxdy}, \qquad (4)$$

where **n** is the unit vector normal to the boundary. This suggests that the budget terms may be sensitive to the location of the boundary. To test the robustness of the results, the budget analysis is done for a $3° \times 3°$ box. While the areal averages of the net vorticity tendency and the nonadvective term decrease proportionally with the increase of the box area [the denominator in Eq. (4)], the $3° \times 3°$ box average of the advective term is comparable to the $2° \times 2°$ box average (not shown). The vertical structure and temporal evolution of each term in the vorticity budget equation remains qualitatively the same. Since vorticity and diabatic heating (related to the tendency term and nonadvective term, respectively) tend to be spatially confined near the pouch center, the large values of the vorticity tendency and the nonadvective term are captured by the $2° \times 2°$ box. By contrast, the low-level inflow, which is related to the advective term, is rather extensive (see Fig. 5 in Part II), so the advective term outside the $2° \times 2°$ box is not negligible. The box average of the residual term, which largely balances the advective term, is also relatively insensitive to the size of the box. This suggests that the various contributions to the vorticity tendency are scale dependent: the immediate effects of tilting due to cloud updrafts is more local compared to the influence of the Eliassen circulation, the influence of which extends to greater distances horizontally.

6. Conclusions

The formation of pre–Hurricane Felix was simulated using the WRF model with a high-resolution configuration sufficient to represent both wave and cloud system processes. Felix originated from an African easterly wave. As demonstrated in the observational study of DMW09, the parent easterly wave of a developing protovortex contains a cyclonic critical layer ''cat's eye'' circulation or a ''wave pouch'' that favors deep convection and protects the protovortex from hostile exterior influences. Although a pouch was present at 600 hPa three days prior to the genesis of Felix in the comoving frame of reference, it was shallow at the beginning of the numerical simulation. The evolution of the Lagrangian flow suggests that the convergence associated with the ITCZ helped to enhance the wave signal and extend the wave pouch from the jet level to the top of the atmospheric boundary layer.

In the numerical simulation the wave pouch is a region of cyclonic rotation and weak strain/shear deformation that protects the moist air inside from dry air intrusion. The pouch provides a moisture- and vorticity-rich environment for VHT activity, and its center serves as a focal point for upscale vorticity aggregation. In this sense, the preferred location of genesis is consistent with the numerous observational cases documented in DMW09. Our high-resolution numerical simulation provides many mesoscale details not accessible to the observational analysis. The storm forms at the pouch center via diabatic vortex merger and system-scale convergence of ambient cyclonic vorticity and vortical remnants.

Analysis of the vorticity evolution using the flux form of the vertical vorticity equation shows that vorticity is initially concentrated at the jet level at the wave stage. Low-level convergence intensifies vorticity near the surface until it becomes stronger than that above, which gives the appearance of a downward migration of the vorticity maximum. The surface circulation is intensified further by deep convection, while the midlevel convergence helps to increase the midlevel vorticity and build a tropospheric-deep vortex.

The apparent downward development of vorticity does not require downward advection of vorticity. Nor is downward development synonymous with a ''top-down'' development from the midtroposphere, as conceived by other authors. Our use of ''downward'' here conveys the idea of pouch development from the easterly jet level (600–700 hPa) to the top of the atmospheric boundary layer. Dry critical-layer processes alone cannot account for TC genesis (DMW09). The Felix case illustrates that deep convection is important, not only for the eventual concentration of cyclonic vorticity in the tropical cyclone, but also to extend the wave pouch downward to the boundary layer, enhancing its role in subsequent development. A complementary role of the boundary layer convergence in the ITCZ for enhancing pouch development was also highlighted in this case.

The formation of Felix in the model simulation supports the hypotheses proposed by DMW09. It is shown that the wave pouch (or the cat's eye of the parent wave's critical layer), as a closed circulation with abundant moisture

and cyclonic rotation, provides a direct pathway for the bottom-up development in the control numerical simulation analyzed herein. It should be pointed out that the wave pouch, a meso-α scale closed circulation, is by nature different from the midlevel meso-β scale convective vortex. The former forms from the nonlinear interaction between a wave and the basic flow and is confined to the lower troposphere, as the wave is; the latter forms within the stratiform region and is confined near the middle levels (~500 hPa, depending on the diabatic heating profile). The formation of Felix in the numerical simulations supports the notion that bottom-up development in the wave pouch is a more efficient and direct route to genesis, as suggested by DMW09.

In a companion study (Montgomery et al. 2009), we examined the wave-to-vortex transition process in an idealized modeling framework. The results of the idealized study also support the key elements of the hypotheses proposed in DMW09 by demonstrating the existence of a region of strong cyclonic vorticity, weak strain, and high saturation fraction within the parent wave's pouch. Similar to the current study, this localized region within the wave pouch serves as the ''attractor'' for an upscale, ''bottom up'' development process while the wave and pouch move together.

Idealized and realistic simulations, and supporting observational evidence, confirm the first and second hypotheses of DMW09 and begin to shed light on how diabatic activation of the parent wave, by a convecting protovortex within, helps to maintain the wave and thereby aid the storm development sequence (H3). Part II discusses in more detail the morphology of convection and model sensitivities.

Acknowledgments. This research was supported by the National Science Foundation (Grants ATM-0733380, ATM-0715426, and ATM-0851554), the Office of Naval Research (Grant N001408WR20129), the National Aeronautics and Space Administration (MIPR NNG07HU171 and Contract NNH04CC63C) and the Naval Postgraduate School in Monterey, California. We thank Dr. Kevin Tory for his constructive comments on an earlier version of the manuscript, Dr. Michael Riemer for providing a trajectory sketch in Fig. 3, and NCAR/CISL for providing computing resources.

REFERENCES

Bolton, D., 1980: The computation of equivalent potential temperature. *Mon. Wea. Rev.,* **108,** 1046–1053.

Dudhia, J., 1989: Numerical study of convection observed during the winter monsoon experiment using a mesoscale two-dimensional model. *J. Atmos. Sci.,* **46,** 3077–3107.

Dunkerton, T. J., 2006: A tale of two ITCZs—The Jim Holton perspective. *Bull. Amer. Meteor. Soc.,* **87,** 1492–1495.

——, M. T. Montgomery, and Z. Wang, 2009: Tropical cyclogenesis in a tropical wave critical layer: Easterly waves. *Atmos. Chem. Phys.,* **9,** 5587–5646.

Emanuel, K. A., 1994: *Atmospheric Convection*. Oxford University Press, 580 pp.

Gray, W. M., 1968: Global view of the origin of tropical disturbances and storms. *Mon. Wea. Rev.,* **96,** 669–700.

——, 1998: The formation of tropical cyclones. *Meteor. Atmos. Phys.,* **67,** 37–69.

Hack, J. J., W. H. Schubert, D. E. Stevens, and H.-C. Kuo, 1989: Response of the Hadley circulation to convective forcing in the ITCZ. *J. Atmos. Sci.,* **46,** 2957–2973.

Halverson, J., and Coauthors, 2007: NASA's Tropical Cloud Systems and Processes Experiment: Investigating tropical cyclogenesis and hurricane intensity change. *Bull. Amer. Meteor. Soc.,* **88,** 867–882.

Haynes, P. H., and M. E. McIntyre, 1987: On the evolution of vorticity and potential vorticity in the presence of diabatic heating and frictional or other forces. *J. Atmos. Sci.,* **44,** 828–841.

Hendricks, E. A., M. T. Montgomery, and C. A. Davis, 2004: The role of ''vortical'' hot towers in the formation of tropical cyclone Diana (1984). *J. Atmos. Sci.,* **61,** 1209–1232.

Hong, S.-Y., and J.-O. Lim, 2006: The WRF single-moment 6-class microphysics scheme (WSM6). *J. Korean Meteor. Soc.,* **42,** 129–151.

Houze, R. A., W. C. Lee, and M. M. Bell, 2009: Convective contribution to the genesis of Hurricane Ophelia (2005). *Mon. Wea. Rev.,* **137,** 2778–2800.

Kain, J. S., and J. M. Fritsch, 1990: A one-dimensional entraining/detraining plume model and its application in convective parameterization. *J. Atmos. Sci.,* **47,** 2784–2812.

Karyampudi, V. M., and H. F. Pierce, 2002: Synoptic-scale influence of the Saharan air layer on tropical cyclogenesis over the eastern Atlantic. *Mon. Wea. Rev.,* **130,** 3100–3128.

Landsea, C. W., 1993: A climatology of intense (or major) Atlantic hurricanes. *Mon. Wea. Rev.,* **121,** 1703–1713.

Mapes, B. E., and R. A. Houze, 1995: Diabatic divergence profiles in western Pacific mesoscale convective systems. *J. Atmos. Sci.,* **52,** 1807–1828.

McWilliams, J. C., 1984: The emergence of isolated coherent vortices in turbulent flow. *J. Fluid Mech.,* **140,** 21–43.

Mlawer, E. J., S. J. Taubman, P. D. Brown, M. J. Iacono, and S. A. Clough, 1997: Radiative transfer for inhomogeneous atmospheres: RRTM, a validated correlated-*k* model for the longwave. *J. Geophys. Res.,* **102,** 16 663–16 682.

Montgomery, M. T., and J. Enagonio, 1998: Tropical cyclogenesis via convectively forced vortex Rossby waves in a three-dimensional quasigeostrophic model. *J. Atmos. Sci.,* **55,** 3176–3207.

——, M. E. Nicholls, T. A. Cram, and A. B. Saunders, 2006: A vortical hot tower route to tropical cyclogenesis. *J. Atmos. Sci.,* **63,** 355–386.

——, Z. Wang, and T. J. Dunkerton, 2009: Intermediate and high resolution numerical simulations of the transition of a tropical wave critical layer to a tropical storm. *Atmos. Chem. Phys. Discuss.,* **9,** 26 143–26 197.

Noh, Y., W.-G. Cheon, S.-Y. Hong, and S. Raasch, 2003: Improvement of the *K*-profile model for the planetary boundary layer based on large eddy simulation data. *Bound.-Layer Meteor.,* **107,** 401–427.

Nolan, D. S., 2007: What is the trigger for tropical cyclogenesis? *Aust. Meteor. Mag.,* **56,** 241–266.

Raymond, D. J., C. López-Carrillo, and L. López Cavazos, 1998: Case-studies of developing east Pacific easterly waves. *Quart. J. Roy. Meteor. Soc.,* **124,** 2005–2034.

Reasor, P. D., M. T. Montgomery, and L. F. Boast, 2005: Mesoscale observations of the genesis of Hurricane Dolly (1996). *J. Atmos. Sci.,* **62,** 3151–3171.

Riehl, H., and J. S. Malkus, 1958: On the heat balance in the equatorial trough zone. *Geophysica,* **6,** 503–538.

——, and J. S. Simpson, 1979: On the heat balance in the equatorial trough zone, revisited. *Contrib. Atmos. Phys.,* **52,** 287–305.

Ritchie, E. A., and G. J. Holland, 1997: Scale interactions during the formation of Typhoon Irving. *Mon. Wea. Rev.,* **125,** 1377–1396.

Schecter, D. A., and D. H. E. Dubin, 1999: Vortex motion driven by a background vorticity gradient. *Phys. Rev. Lett.,* **83,** 2191–2194.

Shapiro, L. J., and H. E. Willoughby, 1982: The response of balanced hurricanes to local sources of heat and momentum. *J. Atmos. Sci.,* **39,** 378–394.

Simpson, J., J. B. Halverson, B. S. Ferrier, W. A. Petersen, R. H. Simpson, R. Blakeslee, and S. L. Durden, 1998: On the role of ''hot towers'' in tropical cyclone formation. *Meteor. Atmos. Phys.,* **67,** 15–35.

Sippel, J. A., J. W. Nielsen-Gammon, and S. E. Allen, 2006: The multiple-vortex nature of tropical cyclogenesis. *Mon. Wea. Rev.,* **134,** 1796–1814.

Skamarock, W. C., J. B. Klemp, J. Dudhia, D. O. Gill, D. M. Barker, W. Wang, and J. G. Powers, 2005: A description of the Advanced Research WRF version 2. NCAR Tech. Note NCAR/TN-468+STR, 88 pp.

Tory, K. J., and M. T. Montgomery, 2006: Internal influences on tropical cyclone formation. *Proc. Sixth Int. Workshop on Tropical Cyclones,* San Jose, Costa Rica, World Meteorological Organization, 2.2.

——, and ——, 2008: Tropical cyclone formation: A synopsis of the internal dynamics. Extended abstracts, *28th Conf. on Hurricanes and Tropical Meteorology,* Orlando, FL, Amer. Meteor. Soc., 10A.1. [Available online at http://ams.confex.com/ams/28Hurricanes/techprogram/paper_138062.htm.]

——, ——, and N. E. Davidson, 2006: Prediction and diagnosis of tropical cyclone formation in an NWP system. Part I: The critical role of vortex enhancement in deep convection. *J. Atmos. Sci.,* **63,** 3077–3090.

Wang, C.-C., and G. Magnusdottir, 2005: ITCZ breakdown in three-dimensional flows. *J. Atmos. Sci.,* **62,** 1497–1512.

Wang, Z., M. T. Montgomery, and T. J. Dunkerton, 2009: A dynamically based method for forecasting tropical cyclogenesis location in the Atlantic sector using global model products. *Geophys. Res. Lett.,* **36,** L03801, doi:10.1029/2008GL035586.

——, ——, and ——, 2010: Genesis of pre–Hurricane Felix (2007). Part II: Warm core formation, precipitation evolution, and predictability. *J. Atmos. Sci.,* **67,** 1730–1744.